Virologica Sinica 40 (2025) 613–623

Contents lists available at ScienceDirect

Virologica Sinica

journal homepage: www.keaipublishing.com/en/journals/virologica-sinica
www.virosin.org

Research Article

Rapid and accurate detection of infectious SARS-CoV-2 by viral receptor capture combined with loop-mediated isothermal amplification

Zixiao Yang [a,b], Xinrong Zhou [b,e], Xikui Sun [b], Liu Cao [a], Tiefeng Xu [a,b], Kun Li [b,c], Hongchao Liu [b,e], Yanxi Ji [a], Lihong Liu [b], Konstantin I. Ivanov [b,f], Zhonghan Yang [a], Deyin Guo [b,d,e,*], Chun-Mei Li [a,*]

[a] Center for Infection and Immunity, School of Medicine, Shenzhen Campus of Sun Yat-sen University, Shenzhen, 518107, China
[b] Guangzhou National Laboratory, Guangzhou International Bio-Island, Guangzhou, 510320, China
[c] Institute of Human Virology, Department of Pathogen Biology and Biosecurity, and Key Laboratory of Tropical Disease Control of Ministry of Education, Zhongshan School of Medicine, Sun Yat-sen University, Guangzhou, 510080, China
[d] Department of Infectious Diseases, Third Affiliated Hospital of Sun Yat-Sen University, Guangzhou, 510630, China
[e] State Key Laboratory of Respiratory Disease, National Clinical Research Center for Respiratory Disease, Guangzhou Institute of Respiratory Health, The First Affiliated Hospital of Guangzhou Medical University, Guangzhou, 510182, China
[f] Faculty of Bioengineering and Bioinformatics, Lomonosov Moscow State University, Moscow, 119234, Russia

ARTICLE INFO

Keywords:
Receptor-based capture
RT-LAMP
SARS-CoV-2
Infectious virus particle detection
Transmission and surveillance

ABSTRACT

Rapid and accurate detection of infectious virus particles, not just viral nucleic acid, is essential to avoid unnecessary quarantine and effectively control the spread of viral diseases such as coronavirus disease 2019 (COVID-19), severe acute respiratory syndrome (SARS), and Middle East respiratory syndrome (MERS). Real-time quantitative polymerase chain reaction (RT-qPCR) was the most widely used detection technique during the COVID-19 outbreak. However, it cannot discriminate between intact infectious viruses and surface-distorted, non-infectious virus particles or naked viral RNA. In this study, we present a strategy for the specific detection of infectious coronaviruses by combining viral receptor capture and reverse transcription loop-mediated isothermal amplification (RT-LAMP). We successfully applied this strategy to detect infectious virus particles of the SARS-CoV-2 surrogate virus and the human coronavirus NL63 (HCoV-NL63). Virus particles were first captured on ELISA plates coated with the recombinant human angiotensin-converting enzyme 2 (hACE2) receptor. Viral RNA was then extracted from the particles and detected by RT-LAMP using virus-specific primers. In our experimental setting, the proposed method had a minimum detection limit (LOD) of 90 PFU/mL, sensitivity of 96.2%, and specificity of 100%. Our study provides a proof-of-concept that viral receptor capture combined with RT-LAMP can differentiate infectious coronaviruses from non-infectious virions or naked viral RNA. This paves the way for this virus detection strategy to become a mainstream tool for the management, prevention and control of epidemic coronavirus diseases.

INTRODUCTION

Since the COVID-19 outbreak in 2019, over 600 million people have been diagnosed worldwide, with a profound impact on global health systems and socioeconomic life (Msemburi et al., 2023). It is estimated that COVID-19 was responsible for approximately 15.9 million deaths worldwide in 2020–2021, either directly from the virus or from secondary complications associated with the pandemic (Chen Y. et al., 2020; GBD, 2021 Demographics Collaborators, 2024; Zhou et al., 2020). The causative agent of COVID-19, severe acute respiratory syndrome coronavirus 2 (SARS-CoV-2), is a member of the *Coronaviridae* family, which includes other important human pathogens such as Middle East respiratory

* Corresponding authors.
E-mail addresses: lichm8@mail.sysu.edu.cn (C.-M. Li), guo_deyin@gzlab.ac.cn (D. Guo).

https://doi.org/10.1016/j.virs.2025.06.006
Received 28 March 2025; Accepted 27 June 2025
Available online 1 July 2025

syndrome coronavirus (MERS-CoV) and severe acute respiratory syndrome coronavirus (SARS-CoV). SARS-CoV-2 can spread quickly between humans and animals by droplet, airborne, and contact transmission, particularly in crowded and public spaces (Chen N. et al., 2020; Chia et al., 2020). SARS-CoV-2 has a single-stranded RNA genome that is approximately 30 kilobases in length. It encodes 16 nonstructural proteins, 4 structural proteins, and up to 10 accessory proteins. Structural proteins include the spike (S), envelope (E), membrane (M), and nucleocapsid (N) proteins. The spike (S) protein consists of two subunits, S1 and S2, which are critical for the viral infection cycle (Hurlburt et al., 2022; Li et al., 2003). As its name implies, the receptor-binding domain (RBD) of the S1 subunit binds to the angiotensin-converting enzyme 2 (ACE2) receptor on the host cell surface, and the S2 subunit facilitates viral fusion with the host cell membrane (Niu et al., 2021; Ou et al., 2021).

Rapid, reliable, and cost-effective detection of viral pathogens is critical for epidemic surveillance. A number of molecular diagnostic strategies have been developed for this purpose. These strategies can be broadly classified into three categories: those that detect viral nucleic acids, viral antigens, or antibodies to viral antigens (Peeling et al., 2022; Wiersinga et al., 2020). The most commonly used diagnostic strategy for SARS-CoV-2 is viral RNA detection, which is typically based on RT-qPCR on nasopharyngeal or nasal specimens (Corman et al., 2020). An alternative strategy is the combination of isothermal nucleic acid amplification with various colorimetric detection approaches, allowing real-time viral RNA detection at the point of patient care (point-of--care testing, POCT) outside of the diagnostic laboratory (Kang et al., 2022; Yan et al., 2014). In addition to traditional nucleic acid amplification-based approaches, a new generation of coronavirus RNA detection methods is emerging. One example is the detection system based on modified CRISPR/Cas9 technology, which allows rapid visual detection of SARS-CoV-2 RNA (Zhu et al., 2023). Among traditional testing approaches, the antigen test, which detects specific viral proteins (typically N or S proteins in the case of coronaviruses), has the advantage of simplicity and speed. Rapid antigen tests (RDTs) have been used to detect multiple SARS-CoV-2 variants from upper respiratory tract swabs (Goux et al., 2024) and nanoparticle-based biosensors to detect the S protein of SARS-CoV-2 (Chen et al., 2021). However, antigen tests tend to have lower sensitivity than nucleic acid-based tests. This can lead to false negative results, especially early in the infection when viral titers are low. The antibody test is an alternative to antigen testing that detects specific antibodies in serum to assess a patient's immune and vaccination status. Enzyme-linked immunosorbent assay (ELISA) and lateral flow assay (LFA) have been successfully used to detect SARS-CoV-2 IgM and IgG antibodies in COVID-19 patients (Whitman et al., 2020). However, since most patients with COVID-19 begin to produce IgM and IgG antibodies at least four days after symptom onset, this method is not suitable for early diagnosis of SARS-CoV-2 infection. In addition, the method is prone to false-positive results. Several new detection technologies, such as biological sensor chips, have been described in the literature but they have not yet found widespread application (Alafeef et al., 2020). A major limitation of these methods is that they cannot yet accurately assess the infectivity of the virus (Furukawa et al., 2020; Gandhi et al., 2020). In addition, these methods often involve complex workflows that require specialized equipment and trained personnel, limiting their use in rapid screening and mass testing scenarios.

SARS-CoV-2 enters the host cell by interacting with the cell-surface receptor ACE2 through the S protein on the viral envelope (Hoffmann et al., 2020). Following virus internalization and uncoating, positive-sense single-stranded viral RNA acts as a template for the *de novo* synthesis of viral proteins and genome. These components then assemble into progeny virions that are released by exocytosis, starting a new round of infection (V'kovski et al., 2021). Thus, a virus particle is infectious only if it has an intact envelope structure with functional S protein (Cuevas-Ferrando et al., 2022; Hong et al., 2021; Tian et al., 2018). To determine whether a virus is truly infectious, one should confirm not only the presence of the virus particle itself but also its integrity and functional competence, particularly its ability to bind to host receptors. In addition, infectious viruses must be differentiated from naked viral RNA, empty virions lacking the viral genome, subviral particles, and viral RNA-protein condensates (Lu et al., 2021; Mattei et al., 2016; Wang et al., 2016). The ability to rapidly and accurately detect infectious viruses is critical for epidemic prevention and control (Rothe et al., 2020). Traditional cell culture-based methods, such as tissue culture infectious dose 50 ($TCID_{50}$) or plaque assays, can accurately determine viral infectivity but are complex, time-consuming, and require specialized equipment. For highly pathogenic viruses, they must be performed in a Biosafety Level 3 (BSL-3) laboratory, making them impractical for rapid screening and mass application. Several methods have been developed to overcome these limitations. For example, viability PCR uses photo-activated dyes or platinum compounds to inhibit the amplification of free nucleic acid fragments, thereby detecting intact SARS-CoV-2 virus particles (Puente et al., 2020; Hong et al., 2021; Cuevas-Ferrando et al., 2022; Veugen et al., 2024). Surface-enhanced Raman scattering (SERS) uses the characteristic Raman signals produced by intact SARS-CoV-2 particles to identify those particles that are truly infectious (Peng et al., 2022; Sitjar et al., 2023). Other studies have used magnetic beads coupled with spike protein antibodies to selectively detect intact SARS-CoV-2 particles (Wu et al., 2022) or nanoparticles to adsorb SARS-CoV-2 in water for detection (Zhu et al., 2024). Although these emerging methods can improve the accuracy of detecting infectious SARS-CoV-2 particles, they also have drawbacks such as complex workflows, equipment dependence, long processing times, and low throughput, all of which limit their practical application in epidemic control.

In this study, we developed a rapid, reliable, and user-friendly method to detect infectious SARS-CoV-2 virus particles by combining highly specific ACE2 receptor capture with reverse transcription loop-mediated isothermal amplification (RT-LAMP). The method demonstrated a minimum detection limit (LOD) of 90 PFU/mL, sensitivity of 96.2%, specificity of 100%, and accuracy of 96.8% in our test setting. Building on the lessons learned from the COVID-19 pandemic, we provide a novel solution for real-time detection of infectious SARS-CoV-2 virions at the point of patient care, which may be critical in the event of a new coronavirus disease outbreak.

RESULTS

A surrogate virus mimicking SARS-CoV-2 cell attachment

Because SARS-CoV-2 must be handled in a biosafety level 3 (BSL-3) laboratory, we decided to replace the highly pathogenic SARS-CoV-2 with a safe and effective alternative: the rVSV-eGFP-SARS-CoV-2 surrogate virus. This recombinant pseudovirus has a vesicular stomatitis virus (VSV) genomic backbone but uses the SARS-CoV-2 spike protein for hACE2 receptor binding, mimicking the mechanism of SARS-CoV-2 cell entry (Li et al., 2021; Ding et al., 2022) (Fig. 1A). In addition, the pseudovirus contains a green fluorescent protein (GFP) reporter gene to track infected cells (Ding et al., 2022; Yahalom-Ronen et al., 2020). The sequence of the spike protein in rVSV-eGFP-SARS-CoV-2 corresponds to that of the humanized S protein of the SARS-CoV-2 Wuhan-Hu-1 strain (GenBank: YP_009724390.1).

We evaluated the infectivity of rVSV-eGFP-SARS-CoV-2 by inoculating Vero E6 cells with the pseudovirus and monitoring subsequent infection. After 24 h, the inoculated Vero E6 cells exhibited intense green fluorescence, indicating successful viral infection (Fig. 1B). This result demonstrated that rVSV-eGFP-SARS-CoV-2 can efficiently attach to and infect Vero E6 cells and that GFP expression can serve as a marker of infection. Based on the above, we concluded that rVSV-eGFP-SARS-CoV-2 effectively mimics SARS-CoV-2 attachment to Vero E6 cells and

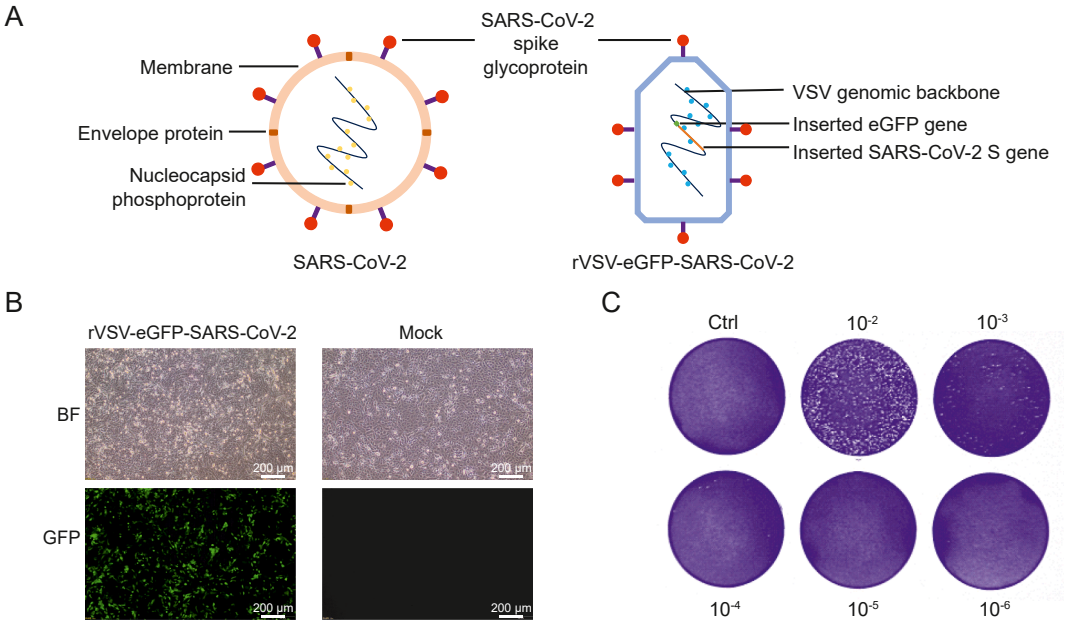

Fig. 1. The surrogate virus rVSV-eGFP-SARS-CoV-2 mimics SARS-CoV-2 cell attachment. **A** Schematic diagram comparing the structure of SARS-CoV-2 and rVSV-eGFP-SARS-CoV-2. **B** rVSV-eGFP-SARS-CoV-2 attaches to and infects Vero E6 cells. Vero E6 cells were infected with rVSV-eGFP-SARS-CoV-2. The cell morphology and GFP fluorescence were observed by bright field (BF) microscopy and fluorescence microscopy at 24 h post infection. Green fluorescence indicates successful infection; no fluorescence was detected in the mock-infected cells. Scale bar, 200 μm. **C** rVSV-eGFP-SARS-CoV-2 is sufficiently infectious for further use in receptor capture assays. Plaque assays were performed with culture supernatants from Vero E6 cells infected with rVSV-eGFP-SARS-CoV-2.

thus provides a suitable testbed for the development of SARS-CoV-2 detection methods.

To further assess the infectivity of the pseudovirus and quantify its titer, we performed a plaque assay. Vero E6 cell monolayers were inoculated with 10-fold serial dilutions of culture supernatants from cells infected with rVSV-eGFP-SARS-CoV-2. After 72 h of incubation, crystal violet staining revealed typical plaque formation (Fig. 1C). The number of plaques showed a strong linear correlation with the pseudovirus titer, which was calculated to be approximately 10^6 PFU/mL. These results demonstrated that rVSV-eGFP-SARS-CoV-2 had sufficient infectivity for further use in receptor capture assays.

Efficient capture of live SARS-CoV-2 surrogate virus by recombinant human ACE2 receptor protein

As a first step toward the development of a receptor capture-based SARS-CoV-2 detection assay, we purified recombinant hACE2 from bacterial cells. For this purpose, we generated a recombinant construct, pET-28a(+)-hACE2, expressing the primary functional domain of hACE2 (the extracellular domain, aa18–740) (Fig. 2A). Double enzyme digestion and DNA sequencing confirmed the presence of the inserted sequence. We then optimized the protein expression conditions to obtain sufficient amounts of recombinant hACE2 protein. As shown in Fig. 2B, while there was no detectable target protein in the uninduced cell lysate (lane 1), we observed significant hACE2 protein expression (the 92 kDa band) upon IPTG induction (lane 2). Following cell lysis with a French press, the protein of interest was found in the centrifugation pellet. The supernatant lacked an obvious target protein band (lane 3), indicating that the recombinant hACE2 protein had aggregated into inclusion bodies (lane 4). The inclusion body problem was successfully solved by dialysis, resulting in protein refolding and increased soluble protein yield (lane 5). Subsequent purification by Ni-NTA affinity chromatography improved the purity of the hACE2 protein to meet the requirements of subsequent experiments (lane 6). Thus, we successfully obtained soluble recombinant hACE2 protein through bacterial expression, dialysis-mediated refolding, and metal chelate affinity chromatography.

As a next step, we validated the results of hACE2 expression and purification by Western blotting (Fig. 2C). We found that the recombinant hACE2 protein could be specifically recognized by the anti-ACE2 antibody, confirming its identity. To assess whether the purified recombinant hACE2 was functionally competent, we examined whether it could compete with endogenous hACE2 for binding to the spike protein on the surface of rVSV-eGFP-SARS-CoV-2 virions. Vero E6 cells were inoculated with a mixture of rVSV-eGFP-SARS-CoV-2 and recombinant hACE2 at increasing concentrations. The efficiency of virus infection was first estimated by observing green fluorescence under a fluorescence microscope (Fig. 2D). The fluorescence intensity was then measured using a microplate reader and analyzed after background subtraction (Fig. 2E). The positive control (no hACE2 added) showed strong fluorescence, confirming that the rVSV-eGFP-SARS-CoV-2 infection was successful. As the concentration of recombinant hACE2 protein increased, the fluorescence intensity gradually decreased, indicating an inhibitory effect on infection. The lowest fluorescence intensity was observed at the highest hACE2 concentration. There was a strong negative correlation between the number of infected cells and the concentration of recombinant hACE2 protein. We concluded that recombinant hACE2 effectively competed with the endogenous receptor, thereby blocking rVSV-eGFP-SARS-CoV-2 cell attachment. Thus, the purified recombinant hACE2 protein was functionally competent and capable of neutralizing rVSV-eGFP-SARS-CoV-2 infection by mimicking the endogenous receptor. Taken together, these results paved the way for the use of recombinant hACE2 in SARS-CoV-2 detection assays based on receptor capture.

Detection of infectious virus particles based on hACE2 receptor capture

To assess the applicability of ACE2 receptor capture for the detection of infectious viruses, we performed RT-qPCR on viral RNA extracted from several viruses after their affinity capture on immobilized recombinant hACE2 protein. Two of these viruses, rVSV-eGFP-SARS-CoV-2 and HCoV-NL63, depend on the ACE2 receptor for cell attachment. The remaining viruses lacked ACE2 binding and/or used an

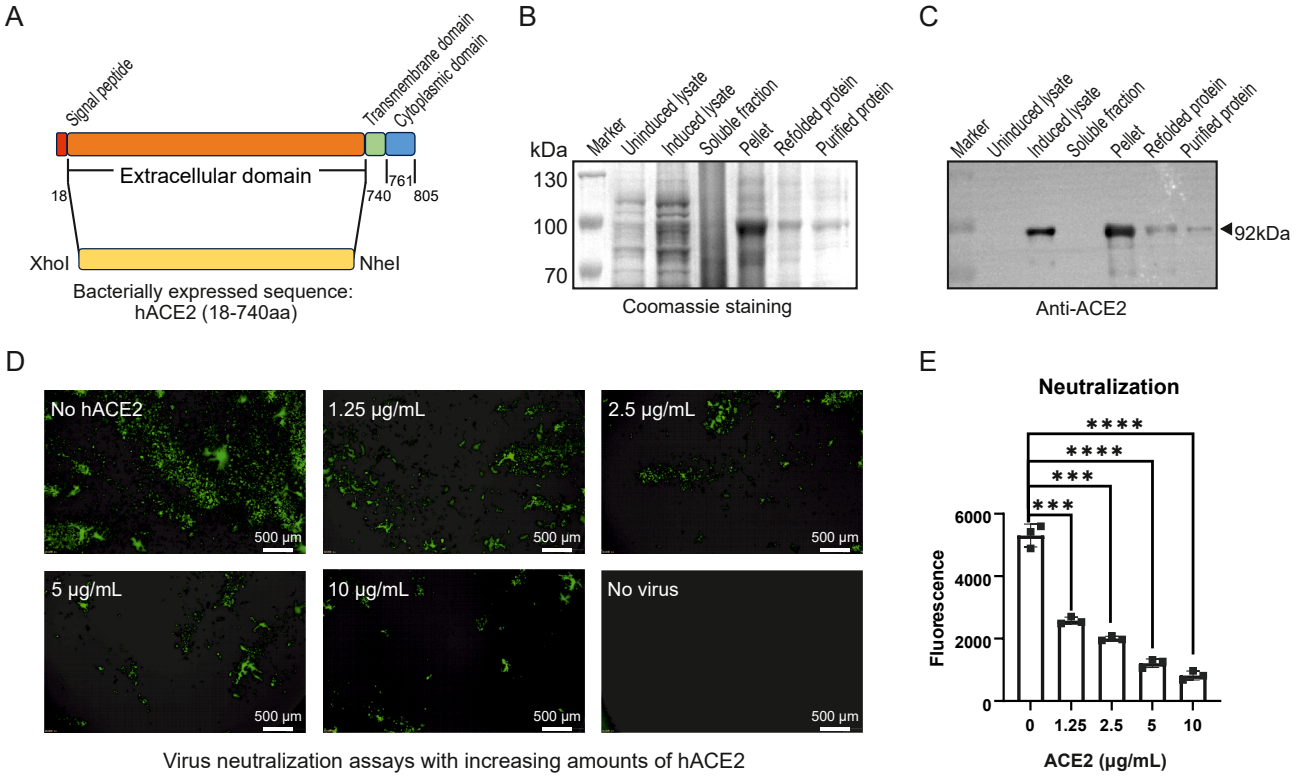

Fig. 2. Purification and functional validation of recombinant hACE2 protein. **A** Cloning strategy for hACE2 expression in *E. coli.* The indicated PCR product was cloned into the pET-28a(+) bacterial expression vector, resulting in the recombinant plasmid pET-28a(+)-hACE2. **B** Bacterial expression and purification of recombinant hACE2 (expected molecular weight ~92 kDa). M: protein marker, 1: uninduced bacterial lysate, 2: bacterial lysate induced with 1 mM IPTG for 6 h, 3: soluble fraction after sonication, 4: pellet after sonication, 5: refolded protein after dialysis, 6: Ni-NTA-purified recombinant hACE2. **C** Bacterially expressed hACE2 is specifically recognized by the anti-ACE2 antibody. Western blot analysis of the same samples as in panel **B**. **D** Virus neutralization assay confirms that the recombinant hACE2 protein is functionally competent. The recombinant protein competes with endogenous ACE2 receptors on the surface of Vero E6 cells for binding to the spike protein, thereby inhibiting viral infection. rVSV-eGFP-SARS-CoV-2 was incubated with increasing amounts of recombinant hACE2 (1.25 μg/mL, 2.5 μg/mL, 5 μg/mL, 10 μg/mL) prior to cell inoculation. No hACE2 was added in the positive control and no virus was added in the negative control. The intracellular GFP expression was assessed by fluorescence microscopy at 48 h post infection. Scale bar, 500 μm. **E** Quantification of fluorescence intensity of infected cells using a microplate reader. As the amount of recombinant hACE2 protein added to rVSV-eGFP-SARS-CoV-2 increased, the number of infected cells decreased accordingly. No hACE2 was added in the control. Statistical analyses were performed using unpaired *t*-test. $^{***}P < 0.001$, $^{****}P < 0.0001$.

ACE2-independent entry mechanism. These included VSV, a SARS-CoV-2 replicon lacking the ACE2-binding spike protein, HCoV-OC43, HCoV-229E, mouse hepatitis virus (MHV)-A59, and porcine delta coronavirus (PDCoV). For each virus, we designed primer pairs targeting the corresponding nucleocapsid (*N*) genes (Supplementary Table S1). Fig. 3A shows representative amplification curves from the RT-qPCR experiments. The Ct values of rVSV-eGFP-SARS-CoV-2 and the positive control were similar, indicating that the recombinant hACE2 receptor effectively captured rVSV-eGFP-SARS-CoV-2. The Ct value of the inactivated rVSV-eGFP-SARS-CoV-2 was significantly lower and similar to that of the negative control, demonstrating that receptor capture can accurately discriminate between infectious and non-infectious viruses. Ct values for viruses defective in ACE2 binding or using an ACE2-independent entry mechanism were also close to background, confirming the specificity of the method. Notably, HCoV-NL63, which specifically binds to the ACE2 receptor, had a Ct value similar to that of rVSV-eGFP-SARS-CoV-2. This suggests that the proposed method can effectively detect not only SARS-CoV-2 or its surrogate but also other coronaviruses that use ACE2 as an entry receptor.

We then focused on the ability of the proposed method to discriminate between infectious and inactivated viruses. We used RT-qPCR to systematically compare the efficacy of ACE2 receptor capture in detecting infectious versus inactivated rVSV-eGFP-SARS-CoV-2. The RT-qPCR analysis revealed that the Ct values in the infectious virus group were consistently and significantly lower than those in the inactivated virus group (Fig. 3B). These results show that the immobilized hACE2 protein could specifically capture the infectious but not the inactivated virus, probably due to its structural defects and impaired activity of the spike protein. Based on the above, we concluded that the proposed method effectively discriminates between infectious and inactivated viruses.

To test whether rVSV-eGFP-SARS-CoV-2 particles captured on the immobilized hACE2 receptor were infectious, we inoculated them into Vero E6 cells and monitored the progress of infection by fluorescence microscopy. The inoculated cells produced strong green fluorescence, confirming successful infection (Fig. 3C). In contrast, no green fluorescence was detected in cells inoculated with a control sample from the receptor capture assay with inactivated virus. These results confirmed that ACE2-captured virus particles were infectious in cultured cells.

Virus stability varies on different surfaces, and viruses gradually lose their infectivity over time (Meister et al., 2022). Therefore, we tested whether the proposed method could track these changes. rVSV-eGFP-SARS-CoV-2 was inoculated onto a paper or glass surface, and infectious virus particles were detected by ACE2 receptor capture at different time points over a 96-h period. Fig. 3D shows that the Ct value increased over time, indicating a gradual loss of viral infectivity. Results became negative after 9 h on paper and 96 h on glass. ACE2 capture assays with inactivated virus always gave negative results ($Ct > 35$), whereas viral RNA collected from the object surface always tested positive ($Ct < 35$). Taken together, these results further support the specificity of the ACE2 capture assay for the detection of infectious virus particles.

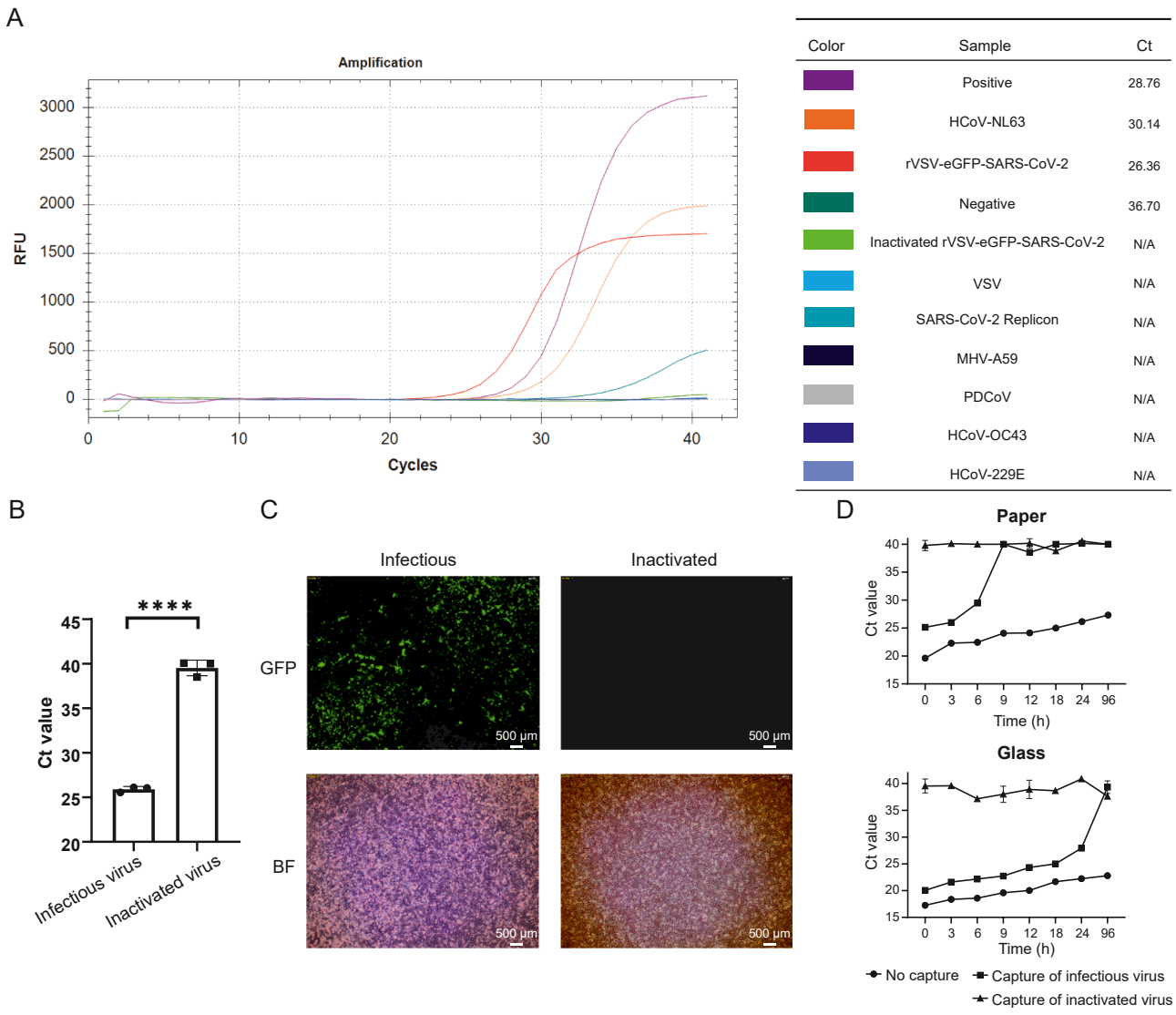

Fig. 3. Detection and infectivity of virus particles captured on immobilized recombinant hACE2 receptor. **A** Representative RT-qPCR amplification curves for the detection of different viruses after ACE2 receptor capture. Only the positive control from the SARS-CoV-2 PCR detection kit, as well as the HCoV-NL63 and rVSV-eGFP-SARS-CoV-2 samples, exhibited clear amplification curves. All other samples were negative with a cycle threshold (Ct) of ≥35, which is commonly used for SARS-CoV-2 detection by RT-qPCR. Note the overlap of several signals close to the baseline. **B** Receptor capture effectively discriminates between infectious rVSV-eGFP-SARS-CoV-2 and inactivated, non-infectious virus. ACE2 receptor-based virion-capture assays were performed with either infectious or inactivated rVSV-eGFP-SARS-CoV-2. The assay results were evaluated by RT-PCR. Statistical analyses were performed using unpaired *t*-test. ****$P < 0.0001$. **C** Validation of viral infectivity in cultured Vero E6 cells. Vero E6 cells were inoculated with infectious rVSV-eGFP-SARS-CoV-2 and inactivated, non-infectious virus. The cell morphology and GFP fluorescence were observed by bright field (BF) microscopy and fluorescence microscopy at 24 h post infection. Green fluorescence indicates successful infection with ACE2-captured rVSV-eGFP-SARS-CoV-2. The absence of fluorescence indicates that the inactivated virus cannot be captured and is not infectious. **D** Stability of rVSV-eGFP-SARS-CoV-2 on different surfaces. A total of 10,000 PFU of rVSV-eGFP-SARS-CoV-2 (untreated or inactivated) was inoculated onto 2 × 2 cm^2 paper or glass surfaces and incubated at room temperature for the indicated times. After ACE2 receptor capture, samples were analyzed by RT-qPCR. In the positive control ("no capture"), the receptor capture step was omitted.

Visual detection using RT-LAMP

Our next goal was to select a rapid, reliable, and cost-effective strategy for detecting receptor-captured viruses that would be suitable for POCT. We chose RT-LAMP over other approaches because it does not require thermal cycling and has a colorimetric readout that allows for immediate visual detection. Specific primer sets (Supplementary Table S2) were designed to amplify viral RNA by RT-LAMP (Fig. 4A). To validate our detection approach, we compared the results of viral RNA amplification using RT-LAMP and conventional RT-PCR. Agarose gel electrophoresis revealed that both RT-PCR (Fig. 4B, left panel) and RT-LAMP (Fig. 4B, right panel) detected RNA from captured rVSV-eGFP-SARS-CoV-2 particles. In the case of conventional RT-PCR, we observed a single band of the correct size (approximately 200 bp). In the case of RT-LAMP, a characteristic ladder of bands indicated successful amplification. No amplification products were detected in the control (receptor capture assay with inactivated virus). As mentioned above, RT-LAMP has an advantage over RT-PCR due to its rapid colorimetric readout. Indeed, Fig. 4C shows that successful RT-LAMP of viral RNA resulted in a decrease in the pH of the reaction mixture, which was visible as a color change of an indicator dye from pink to yellow.

We then tested whether the proposed method was indeed specific for the detection of the SARS-CoV-2 pseudovirus rVSV-eGFP-SARS-CoV-2. We performed the same ACE2 receptor capture assay with RT-LAMP for several viruses, including rVSV-eGFP-SARS-CoV-2, HCoV-NL63, HCoV-OC43, HCoV-229E, MHV-A59, PDCoV, and VSV (Fig. 4D). Only

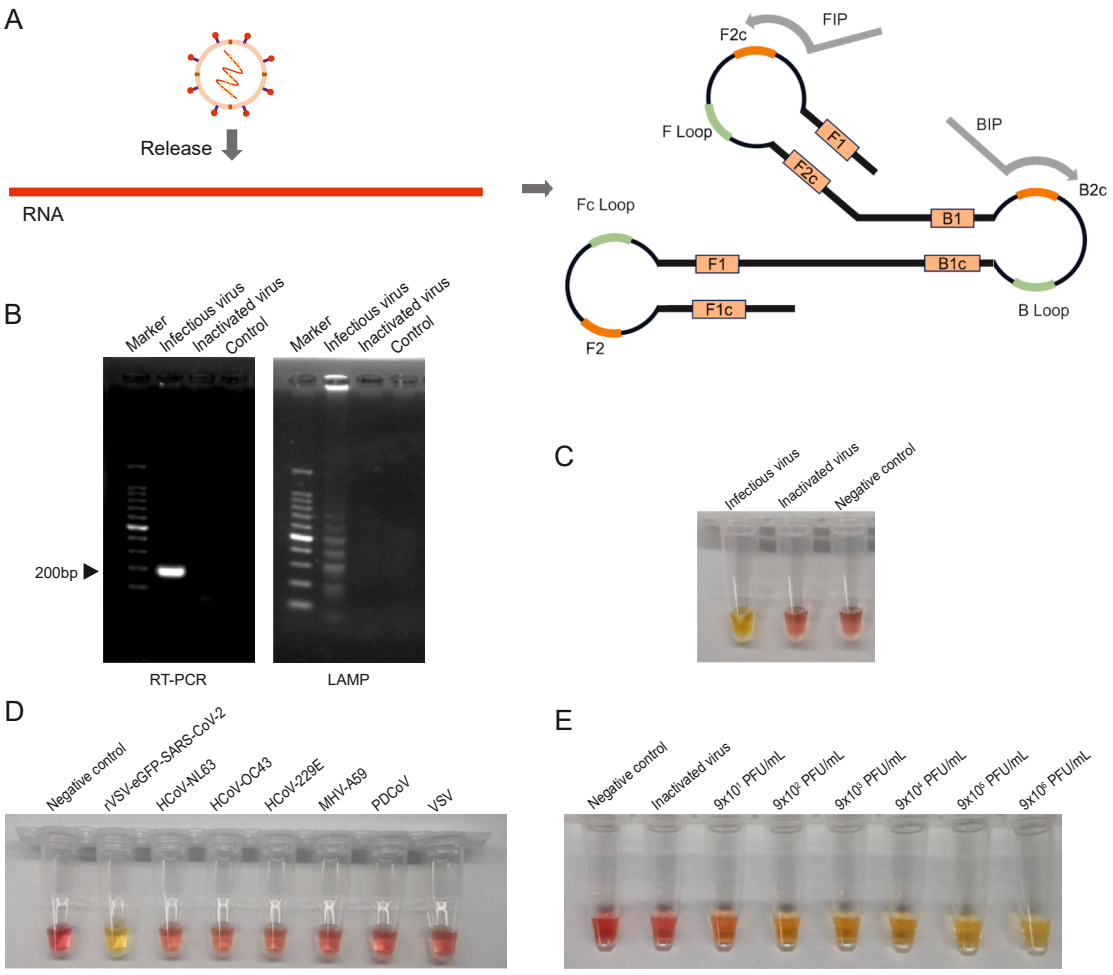

Fig. 4. Detection of virus particles captured on immobilized recombinant hACE2 by RT-LAMP. **A** Schematic diagram illustrating the principle behind detecting viral RNA from affinity-captured virus particles with RT-LAMP. First, the viral RNA is extracted from the receptor-captured virions and transcribed into cDNA using reverse transcriptase. Next, multiple primer sets and Bst DNA polymerase are used to amplify cDNA at a constant temperature. **B** Comparative detection of viral RNA from captured rVSV-eGFP-SARS-CoV-2 particles by RT-PCR (left) and RT-LAMP (right). Amplification products were resolved by agarose gel electrophoresis and visualized by ethidium bromide staining. **C** Colorimetric readout of RT-LAMP reactions after rVSV-eGFP-SARS-CoV-2 capture on immobilized recombinant hACE2. Positive samples appear yellow, while negative samples remain pink. **D** The specificity of ACE2 receptor capture assay with RT-LAMP. Different viruses, including rVSV-eGFP-SARS-CoV-2, HCoV-NL63, HCoV-OC43, HCoV-229E, murine hepatitis virus strain A59 (MHV-A59), porcine deltacoronavirus (PDCoV), and vesicular stomatitis virus (VSV) (9×10^5 PFU), were tested with the same measurement. The sample with no added virus was used as a negative control. Note that ACE2 receptor capture followed by RT-LAMP detects rVSV-eGFP-SARS-CoV-2 but not other viruses. **E** Determination of the detection limit (LOD) for the ACE2 receptor capture/RT-LAMP assay.

the sample containing rVSV-eGFP-SARS-CoV-2, which requires ACE2 for cell entry, tested positive (yellow). All other virus samples tested negative (pink), demonstrating the specificity of the proposed method. To evaluate the sensitivity of the method, we performed receptor capture assays with RT-LAMP for six serial 10-fold dilutions of rVSV-eGFP-SARS-CoV-2, ranging from 9×10^6 PFU/mL to 9×10^1 PFU/mL (Fig. 4E). At low viral titers, it took approximately 30 min for the color of the reaction mixture to change from pink to yellow. However, when the viral titer exceeded 10^4 PFU/mL, the color change occurred much faster (within 15–20 min). As shown in Fig. 4E, the established method had a detection limit (LOD) of 90 PFU/mL. Negative virus-free controls and inactivated virus samples processed with receptor capture with did not change color and remained pink.

Validation of the proposed method for detecting infectious virus particles

To test the influence of sample matrix on receptor capture and amplification, we spiked saliva samples and environmental surface swabs with 5000 PFU of rVSV-eGFP-SARS-CoV-2. Then, we performed receptor capture experiments followed by virus detection using either LAMP or RT-qPCR. We observed no effect of the sample matrix on virus detection by either method. Both methods successfully detected infectious virus particles in the samples (Fig. 5A and B). These results are consistent with the previously published data showing that affinity capture-based methods can accurately and reliably detect SARS-CoV-2 in clinical samples (Dignan et al., 2021; Rabe et al., 2025).

To further evaluate the performance of the proposed detection method, serial dilutions of rVSV-eGFP-SARS-CoV-2 were employed. A total of 32 samples were prepared and divided into seven groups. The first group contained control samples (0 PFU), while the remaining six groups contained samples with increasing pseudovirus titers (90 PFU/mL, 9×10^2 PFU/mL, 9×10^3 PFU/mL, 9×10^4 PFU/mL, 9×10^5 PFU/mL, and 9×10^6 PFU/mL; Fig. 5C). Virion detection was performed using hACE2 receptor capture combined with RT-LAMP, and the colorimetric assay results were visually observed with the naked eye: negative (−) samples remained pink, while positive (+) samples turned yellow. As shown in Fig. 5D, the assay results correlated well with viral titers. Samples with high viral titers (9×10^4 PFU/mL and above) exhibited a consistent, bright yellow color. In the medium titer group

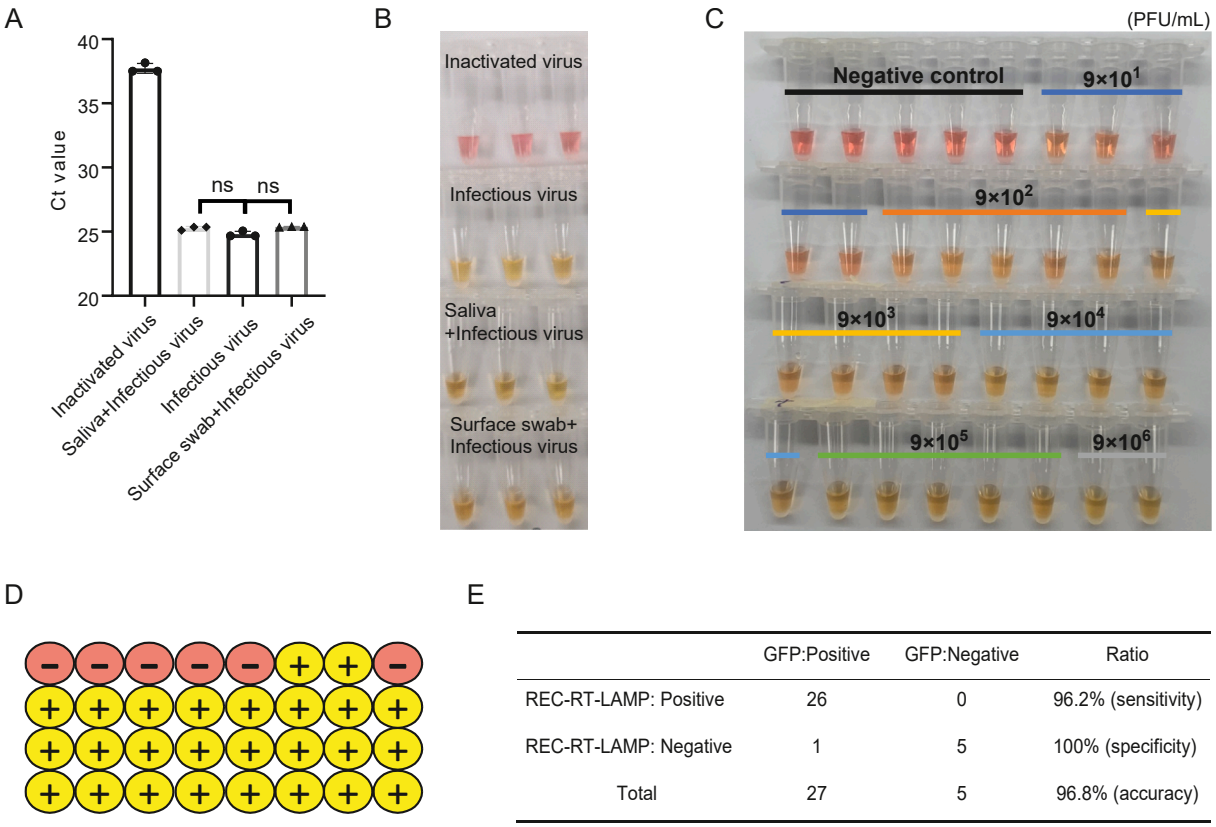

	GFP:Positive	GFP:Negative	Ratio
REC-RT-LAMP: Positive	26	0	96.2% (sensitivity)
REC-RT-LAMP: Negative	1	5	100% (specificity)
Total	27	5	96.8% (accuracy)

Fig. 5. Validation of a diagnostic test prototype based on coronavirus capture and RT-LAMP. **A** The sample matrix does not affect the results of ACE2 receptor capture assays followed by virus detection by RT-qPCR. Saliva samples and environmental surface swabs spiked with infectious rVSV-eGFP-SARS-CoV-2 were analyzed alongside the infectious virus alone. Statistical analyses were performed using unpaired *t*-test. ns: $P > 0.05$. **B** Similar results were obtained with ACE2 receptor capture combined with LAMP. Colorimetric analysis showed no difference in the detection of the infectious virus alone or the infectious virus mixed with saliva or surface swabs. **C** Results of the ACE2 receptor capture/RT-LAMP assay with simulated clinical samples containing increasing amounts of rVSV-eGFP-SARS-CoV-2. **D** Schematic representation of the assay results in panel **C**, with pink indicating negative (−) and yellow indicating positive (+) results. There was one false negative result (tube 8). **E** Diagnostic performance of the proposed test (sensitivity, specificity, and accuracy). REC-RT-LAMP: receptor capture RT-LAMP.

(9×10^2, 9×10^3 PFU/mL), all samples tested positive but the color was darker. Finally, in the low titer group (90 PFU/mL), 4 out of 5 samples showed a faint color change but one sample showed no positive signal. This false-negative result was most likely caused by insufficient virus particle capture efficiency and/or sensitivity of RT-LAMP to detect low-copy RNA (approaching the detection limit). Statistical analysis of 32 simulated samples showed that the detection system had an overall accuracy of 96.8%, a sensitivity of 96.2% (26 of 27 positive samples were correctly detected), and a specificity approaching 100% (all five negative samples were correctly detected) (Fig. 5E). Overall, ACE2 receptor capture combined with RT-LAMP demonstrated high accuracy and reliability, making it a viable option for detecting infectious virus particles in clinical and community samples.

DISCUSSION

This study describes a novel method based on ACE2 receptor capture and RT-LAMP for the detection of infectious coronaviruses that use ACE2 as an entry receptor. Unlike traditional RT-qPCR-based methods that detect both enveloped and naked viral RNA, the proposed method is selective for intact infectious virions capable of cell attachment. The method has demonstrated high sensitivity (96.2%) and specificity (approaching 100%) for the detection of infectious viruses. In addition, the use of rapid amplification and colorimetric detection allows visual assessment of results in much less time than traditional cell culture-based virus detection methods.

Conventional nucleic acid detection methods such as RT-qPCR, while highly sensitive and specific, can only detect the presence of viral RNA without confirming its origin. Positive RT-qPCR results can be obtained not only from intact infectious virions, but also from non-infectious particles defective in cell attachment or naked RNA fragments, making it difficult to assess the true risk of infection. As a result, differentiating infectious from non-infectious viruses remains a significant challenge in virus detection. In this study, we developed a method for the selective detection of infectious coronavirus particles capable of cell attachment and entry. The method is based on the selective retention of virus particles on the immobilized ACE2 receptor protein, simulating virus attachment to the host cell surface, a critical step in the SARS-CoV-2 infection cycle. Another key feature of the proposed method is the use of RT-LAMP, which enables rapid reverse transcription and amplification under isothermal conditions. RT-LAMP does not require expensive equipment, and the colorimetric results can be interpreted visually with the naked eye, making the proposed method suitable for resource-limited testing scenarios.

Despite the above advantages, the proposed method has several limitations. For samples with high viral titers, the colorimetric reaction was fast and the signal was easily detectable. At such high viral titers, a diagnostic test based on the proposed method will have sufficient sensitivity and specificity, and the results will be easy to interpret. However, for samples with low viral titers, the sensitivity of the diagnostic test may be insufficient. At these low viral titers, a number of problems may occur, including partial target loss during sample

recovery, decreased capture efficiency, and reduced amplification efficiency (Cuevas-Ferrando et al., 2022). All of these factors can produce false negatives or weak positives. This phenomenon is well documented in environmental monitoring and contaminant detection. Environmental samples may contain so little virus that pre-enrichment is required. Certain contaminants may also be present that interfere with the amplification process or alter the pH, reducing capture efficiency (Plante et al., 2024; Tian et al., 2010; Zhu et al., 2024). Therefore, the proposed method will require further optimization to improve its ability to process samples with low viral titers. This can be achieved by improving receptor capture, amplification efficiency, and monitoring techniques, as well as by introducing additional purification and/or sample pretreatment steps. Another limitation of the proposed method in real-world applications is the high sensitivity of RT-LAMP, which makes it susceptible to carryover contamination. Aerosol spread within the laboratory can lead to accumulative contamination and false positive results (Huang et al., 2020). In addition, relying solely on visual inspection to interpret colorimetric results can lead to misinterpretation. Standardizing the colorimetric assay using automated readers is a viable option, but it would require additional equipment and introduce more steps (Davidson et al., 2021). Finally, it should be noted that due to resource constraints, the proposed method has not yet been validated with live SARS-CoV-2 and clinical samples from COVID-19 patients (e.g., nasopharyngeal swabs). Although experimental results with the SARS-CoV-2 surrogate virus and HCoV-NL63 have demonstrated the method's efficacy and application potential, the complexity of real-world samples (e.g., viral mutations, various types of inhibitors and interfering factors) may place higher demands on the method's performance.

Although the proposed method requires further optimization, it has the potential for a wide range of practical applications, particularly in public health and safety. The speed, efficiency, and convenience of the method already qualify it for POCT, making it a valuable tool for epidemic prevention and control. Furthermore, the method allows the use of different primer sets to detect different viral genotypes (e.g., SARS-CoV-2 variants) or viruses that share the same receptor (e.g., HCoV-NL63 and SARS-CoV). Finally, by replacing the ACE2 receptor with receptors specific for other coronaviruses, the method can be used to detect a variety of other important human pathogens, such as MERS-CoV (Selvaraj et al., 2019).

CONCLUSIONS

In the present study, we developed a method for selective detection of infectious coronavirus particles based on ACE2 receptor capture combined with RT-LAMP. The method can discriminate among infectious virions, surface-distorted and non-infectious virions, and naked viral RNA based on affinity for the ACE2 entry receptor. Colorimetric detection enables direct visual interpretation of test results, achieving 100% specificity, 96.2% sensitivity, and 96.8% accuracy in our experimental conditions. The proposed method has several advantages over other existing methods, such as RT-PCR and antibody-based methods, in terms of speed, ease of use, and equipment dependence. Most importantly, the method is suitable for detecting infectious coronaviruses at the point of patient care, which may be urgently needed in the event of a new coronavirus disease outbreak.

MATERIALS AND METHODS

Cells and viruses

The HEK-293T (ATCC: CRL-11268), Vero E6 (ATCC: CRL-1586), LLC-PK1 (ATCC: CL-101), and HRT-18 (ATCC: CCL-244) cells were originally obtained from the American Type Culture Collection (ATCC) and maintained in our laboratory. The 17Cl-1 (RRID: CVCL_VT75) and Huh7 (RRID: CVCL_0336) cell lines were kindly provided by Dr. Yuzheng Zhou (Shenzhen Third People's Hospital, the Second Affiliated Hospital, School of Medicine, Southern University of Science and Technology) and Prof. Jincun Zhao (Guangzhou National Laboratory), respectively. The cells were cultured in Dulbecco's modified eagle medium (DMEM) supplemented with 10% fetal bovine serum (FBS, #10099141C, Gibco), penicillin (100 U/mL), and streptomycin (0.1 mg/mL) at 37 °C in a humidified atmosphere of 5% CO2. Human coronavirus NL63 (HCoV-NL63, RefSeq:NC_005831), human coronavirus OC43 (HCoV-OC43, RefSeq:NC_006213), human coronavirus 229E (HCoV-229E, RefSeq:NC_002645), murine hepatitis virus strain A59 (MHV-A59, RefSeq:NC_048217), porcine deltacoronavirus (PDCoV, GenBank:MW685623), and rVSV-eGFP-SARS-CoV-2 (Li et al., 2021; Ding et al., 2022) recombinant pseudovirus (provided by Professor Aihua Zheng from the Institute of Zoology, Chinese Academy of Sciences) were propagated in susceptible cell lines in virus culture medium (DMEM with 2% FBS) and the supernatants were stored at −80 °C for later use. Their infectivity was determined by conventional titration and/or fluorescence intensity measurement. The replicon was reported in our previous work (Jin et al., 2021). All experiments involving viruses were performed in a biosafety level 2 (BSL-2) laboratory, following the appropriate biosafety protocols.

Antibodies and reagents

The following antibodies and reagents were used: ACE2 monoclonal antibody (#66699-1-IG, Proteintech), goat-Mouse IgG (H&L) (HRP conjugate) (#511103, ZenBio), ExFect Transfection Reagent (#T101-02, Vazyme), ECL chemiluminescent substrate (#180–5001, Tanon), E.Z.N.A.® Viral RNA Kit (#R6874, OMEGA), SARS-CoV-2 nucleic acid 356 detection kit (#DA0992, Daan Company), WarmStart Colorimetric LAMP 2x Master Mix (DNA & RNA) (#M1800, New England Biolabs), TB Green® Premix Ex Taq™ II FAST qPCR (#CN830A, Takara), RT MASTER MIX takara (#RR036A, Takara), tetramethylethylenediamine (TEMED) (#T22500, Sigma), sodium dodecyl sulfate (SDS) (#BS088, Biosharp), ammoniumpersulfate (APS) (#A3678, Sigma).

Plaque assay

Plaque assay was used to determine the infectious titer of the pseudovirus as previously described (Yahalom-Ronen et al., 2020). Briefly, Vero E6 cells were plated at a density of 1×10^5 cells per well in a 6-well plate. When the cells reached 90%–100% confluence, 10-fold serial dilutions of the rVSV-eGFP-SARS-CoV-2 pseudovirus were prepared by diluting virus stock with cell culture medium. After removing cell culture medium from the 6-well plates, 500 μL of the diluted virus solution was added to each well to infect the Vero E6 cell monolayer. The plate was gently agitated to ensure uniform virus distribution and then incubated at 37 °C for 2 h to promote virus adsorption. Unbound virus was removed, and the wells were washed with 1 mL sterile PBS. Overlay medium (2 mL/well, DMEM with 0.8% methylcellulose and 2% FBS) was added and the cells were incubated at 37 °C, 5% CO_2 for 72 h to allow plaque formation. Then, 1 mL of 0.5% crystal violet solution containing 25 μL 40% polyformaldehyde, 5 μg crystal violet and 37.5 μL ethanol was added to each well. The cells were fixed and stained for 4 h at room temperature. The number of plaques was then counted and viral titers were recorded as PFU/mL. For replicate experiments requiring equal virus titers, the virus solutions were concentrated using the Universal Virus Concentration Kit (#C2901L, Beyotime).

Western blot analysis

Western blot analysis was performed as previously described (Lin et al., 2022). Briefly, protein samples were mixed with 5x SDS-PAGE protein sample loading buffer (#P0286, Beyotime, China) and heated at 95 °C for 10 min. Denatured samples were loaded onto an SDS-PAGE gel (5% stacking gel and a 10% resolving gel with a Tris-glycine buffer

system). Electrophoresis was performed for 30 min at 90V, followed by 90 min at 120V. After electrophoresis, proteins were transferred to a 0.22 μm PVDF membrane (Millipore, USA) using a wet transfer system at 280 mA for 120 min. Following blocking for 1 h in PBST containing 5% skimmed milk, the membrane was incubated overnight at 4 °C with mouse anti-human ACE2 antibody (#ab108209, Abcam, UK). The immunoblot was visualized using the ChemiDoc MP system (Bio-Rad).

Prokaryotic expression and purification of the SARS-CoV-2 receptor ACE2

Human ACE2 (GenBank: ON637243.1), the specific receptor for SARS-CoV-2, is composed of 805 aa, including a signal peptide (1–17 aa), an extracellular domain (18–740 aa), a transmembrane domain (741–761 aa), and a cytoplasmic domain (762–805 aa). The extracellular domain, which is the main functional region, was amplified with specific primers (forward primer: 5′-CTAGCTAGCCAGTCCACCATTGAGGAACAGG-3′, reverse primer: 5′-CCGCTCGAGACTTCAGTTCTAGGAATGATATCAGACAC-3′) from the pEF6-ACE2-MycHis plasmid template. The amplified hACE2 DNA fragment was purified and double digested with *Xho*I and *Nhe*I restriction enzymes, and the product was subsequently ligated into the pET-28a(+) vector, resulting in the recombinant plasmid pET-28a(+)-hACE2. The DNA sequence of ACE2 was verified by sequencing. The recombinant plasmid pET-28a(+)-hACE2 was transformed into E. coli Rosetta (DE3) cells. Protein expression was performed in 250 mL LB medium supplemented with 50 μg/mL kanamycin. When the absorbance OD600 nm reached 0.6–0.8, 1 mM isopropyl β-D-1-thiogalactopyranoside (IPTG) was added to induce target protein expression. After 6 h of induction at 37 °C, cells were harvested and lysed using a French press. The expressed protein was purified by affinity chromatography on Ni-NTA agarose resin. The bound ACE2 was eluted with 1 × NTA buffer containing 20 mM–250 mM imidazole in 8 M urea. The fractions containing ACE2 were collected and dialyzed against a urea gradient (4, 2 and 0 M in NTA buffer) and finally PBS. The protein was further purified by gel filtration using the AKTA Pure System (Cytiva, AKTA Pure), sterilized by filtration, and stored in PBS at −80 °C.

Pseudovirus-based neutralization assay

Pseudovirus-based neutralization assay (PBNA) was performed as previously described (Ju et al., 2020). The steps were as follows: 10 μL of pseudovirus solution containing 1×10^2 PFU was mixed with an equal volume of serial dilutions of 0.2 mg/mL hACE2 protein stock and incubated at 37 °C for 1 h. The mixtures were added to a 96-well plate pre-seeded with Vero E6 cells and incubated for 48 h. A mixture containing pseudovirus without hACE2 served as the positive control, while uninfected cells served as the negative control. After incubation, intracellular GFP expression was assessed by fluorescence microscopy. Fluorescence intensity was measured with a fluorometer (SynergyH1, BioTek). The neutralizing effect of the ACE2 protein was calculated by comparing the fluorescence intensity between treatment groups, allowing for the assessment of the effect of hACE2 in PBNA (Tan et al., 2020).

Surface swabbing

Viral stock was serially diluted 10-fold in sterile PBS to prepare 1 mL of each titer (ranging from 9×10^1 to 10^6 PFU/mL). Virus inactivation was achieved by incubation at 95 °C for 5 min. Different surfaces (glass and paper), each measuring 2 × 2 cm, were artificially contaminated with 10 μL of virus solutions (1×10^6 PFU/mL). The surfaces were then allowed to air-dry at room temperature for 30 min to simulate virus exposure to environmental conditions. The swab sampling procedure was performed as follows: First, the surface was swabbed unidirectionally five times with a PBS-moistened swab. The swab was then transferred to a microtube containing 300 μL PBS and vortexed to release the virus. The entire procedure was repeated three times. All steps were performed in a contamination-free environment, and samples were stored on ice for further analysis.

ACE2-based virus capture and infectivity assay

rVSV-eGFP-SARS-CoV-2 infectious virus particles were captured on the immobilized hACE2 receptor. First, 100 μL of 2 μg/mL hACE2 protein solution was added to ELISA plates (FEP101296, Biofil) and incubated at 4 °C for 6 h to allow the protein to bind to the plate surface. The protein solution was removed from the plates and the wells were washed once with PBST (PBS, pH 7.4, with 0.05% Tween-20). The wells were blocked with 5% bovine serum albumin (BSA) in PBS for 2 h at room temperature. The blocking solution was removed and the wells were washed three times with PBST. The test sample (100 μL) — either an environmental swab, a purified virus solution, or an infected cell culture medium — was added to the wells and incubated for 30 min at room temperature to ensure sufficient virus binding to the immobilized hACE2. The wells were washed three times with PBST to remove contaminants and unbound virus particles. The performance of the virus capture platform was validated using positive controls (pseudoviruses of known titer) and negative controls (virus-free samples). Infectivity of captured viruses was validated in cultured cells by detecting GFP fluorescence.

Viral RNA extraction

Viral RNA extraction was performed according to the manufacturer's instructions (E.Z.N.A.® Viral RNA Kit, #R6874, Omega Biotek). The procedure consisted of four steps: sample lysis, RNA binding, washing, and elution. First, samples were thoroughly mixed with QVL Lysis Buffer and allowed to stand for 5 min to ensure complete lysis. After lysis, anhydrous ethanol was added to assist RNA binding to the column. The sample was loaded onto the column and centrifuged at 12,000×*g* for 30 s. The column was washed once with VHB buffer and twice with RNA Wash Buffer II to remove proteins and other contaminants. To elute RNA, 20 μL RNase-free water was added directly to the center of the column, incubated for 1 min, and centrifuged. The resulting RNA was used immediately or stored at −80 °C for later use.

Reverse transcription quantitative PCR (RT-qPCR)

Viral RNA was quantified by RT-qPCR using primers targeting the nucleocapsid (*N*) gene. Primers were designed using Primer Explorer and Oligo 7 software. Primer sequences are listed in Supplementary Table S1. The extracted RNA was reverse transcribed with Vazyme reverse transcriptase (Nanjing, China) using a SimpliAmp™ thermal cycler (Thermo Fisher Scientific). The mixture containing 5× RT Mix and RNA template was incubated at 37 °C for 15 min and then at 85 °C for 5 s qPCR was performed using Takara SYBR Green Master Mix. PCR reactions were carried out in a Bio-Rad CFX384 thermocycler as follows: initial denaturation at 95 °C for 30 s followed by 40 cycles of DNA amplification, each consisting of a 5-s segment at 95 °C and a 10-s segment at 60 °C. Amplification curves were analyzed using CFX Manager software. Each reaction set included positive, negative, and blank controls.

Reverse transcription loop-mediated isothermal amplification (RT-LAMP)

RT-LAMP was used for rapid colorimetric detection of receptor-captured virus particles. RT-LAMP primers were designed using Primer Explorer software (version 5). The resulting primer set targeted the *N* gene of vesicular stomatitis virus (VSV) (GenBank: NC_001560.1) and consisted of six primers: two outer primers (F3 and B3), two loop primers (LF and LB), and two inner primers (FIP and BIP). The primer sequences are listed in Supplementary Table S2. Each well of an ELISA plate contained 20 μL of the receptor-captured virus sample in

RNase-free water. The plate was sealed to prevent evaporation and viral RNA was released from the captured virions by thermal lysis. This was achieved by heating the samples to 95 °C for 5 min followed by cooling to room temperature. 1 μL of the resulting viral RNA template was mixed with 12.5 μL of WarmStart colorimetric LAMP 2× Master Mix, 2.5 μL primer mix, and 9 μL RNase-free water. The mixtures were transferred to PCR tubes, sealed to prevent evaporation and incubated at 65 °C for 30 min. The color change from pink to yellow indicated successful amplification. The results were confirmed by visual observation or colorimetric analysis (Li et al., 2022).

Statistical analysis

Statistical analysis was performed using GraphPad Prism 8 software. The differences between the captured infectious and inactivated viruses were analyzed using an unpaired *t*-test. Each assay included at least two biological replicates and three technical replicates. $*P < 0.05$, $**P < 0.01$, $***P < 0.001$, $****P < 0.0001$; ns, $P > 0.05$.

DATA AVAILABILITY

All data relevant to the study are included in the article. The raw data are available upon request.

ETHICS STATEMENT

This study does not include any results from human or animal subjects. All virological experiments involving the rVSV-eGFP-SARS-CoV-2 surrogate virus, HCoV-NL63, and other reference coronaviruses were performed exclusively in certified Biosafety Level 2 laboratories at the Guangzhou National Laboratory and Sun Yat-sen University. These experiments were conducted in accordance with institutional biosafety regulations and the WHO Laboratory Biosafety Manual.

AUTHOR CONTRIBUTIONS

Zixiao Yang: investigation, methodology, formal analysis, validation, visualization, writing-original draft. Xinrong Zhou: investigation, data curation, resources. Xikui Sun: methodology, validation. Liu Cao: investigation, resources. Tiefeng Xu: formal analysis. Kun Li: methodology. Hongchao Liu: investigation. Yanxi Ji: formal analysis. Lihong Liu: investigation, resources. Konstantin I. Ivanov: visualization, writing-review & editing. Zhonghan Yang: investigation, supervision. Deyin Guo and Chun-Mei Li: conceptualization, methodology, data curation, funding acquisition, project administration, resources, supervision, writing-review & editing.

CONFLICT OF INTEREST

The authors declare that they have no conflict of interest. Prof. Deyin Guo is an editorial board member for *Virologica Sinica* and was not involved in the editorial review or the decision to publish this article.

ACKNOWLEDGMENTS

We thank Prof. Aihua Zheng from the Institute of Zoology, Chinese Academy of Sciences for providing the rVSV-eGFP-SARS-CoV-2 virus. This study was supported by the National Natural Science Foundation of China (32470160), the National Key Research and Development Program of China (2021YFC2300100, GZNL2023A01008), the Shenzhen Science and Technology Program (#JSGG20200225150431472, JSGG20210901145403012, and JSGG20220301090005007), the "Pearl River Talent Plan" Innovation and Entrepreneurship Team Project of Guangdong Province (2016LJ06Y540 and 2019ZT08Y464), and the Science and Technology Program of Guangdong Province, China (2021B1212040017).

APPENDIX A. SUPPLEMENTARY DATA

Supplementary data to this article can be found online at https://doi.org/10.1016/j.virs.2025.06.006.

REFERENCES

Alafeef, M., Dighe, K., Moitra, P., Pan, D., 2020. Rapid, ultrasensitive, and quantitative detection of SARS-CoV-2 using antisense oligonucleotides directed electrochemical biosensor chip. ACS Nano 14, 17028–17045.

Chen, K.-L., Yang, Z.-Y., Lin, C.-W., 2021. A magneto-optical biochip for rapid assay based on the Cotton-Mouton effect of gamma-Fe2O3@Au core/shell nanoparticles. J. Nanobiotechnol. 19, 301.

Chen, N., Zhou, M., Dong, X., Qu, J., Gong, F., Han, Y., Qiu, Y., Wang, J., Liu, Y., Wei, Y., Xia, J., Yu, T., Zhang, X., Zhang, L., 2020. Epidemiological and clinical characteristics of 99 cases of 2019 novel coronavirus pneumonia in Wuhan, China: a descriptive study. Lancet 395, 507–513.

Chen, Y., Liu, Q., Guo, D., 2020. Emerging coronaviruses: genome structure, replication, and pathogenesis. J. Med. Virol. 92, 2249.

Chia, P.Y., Coleman, K.K., Tan, Y.K., Ong, S.W.X., Gum, M., Lau, S.K., Lim, X.F., Lim, A. S., Sutjipto, S., Lee, P.H., Son, T.T., Young, B.E., Milton, D.K., Gray, G.C., Schuster, S., Barkham, T., De, P.P., Vasoo, S., Chan, M., Ang, B.S.P., Tan, B.H., Leo, Y.-S., Ng, O.-T., Wong, M.S.Y., Marimuthu, K., Singapore 2019 Novel Coronavirus Outbreak Research Team, 2020. Detection of air and surface contamination by SARS-CoV-2 in hospital rooms of infected patients. Nat. Commun. 11, 2800.

Corman, V.M., Landt, O., Kaiser, M., Molenkamp, R., Meijer, A., Chu, D.K., Bleicker, T., Brünink, S., Schneider, J., Schmidt, M.L., Mulders, D.G., Haagmans, B.L., van der Veer, B., van den Brink, S., Wijsman, L., Goderski, G., Romette, J.-L., Ellis, J., Zambon, M., Peiris, M., Goossens, H., Reusken, C., Koopmans, M.P., Drosten, C., 2020. Detection of 2019 novel coronavirus (2019-nCoV) by real-time RT-PCR. Euro Surveill. 25, 2000045.

Cuevas-Ferrando, E., Girón-Guzmán, I., Falcó, I., Pérez-Cataluña, A., Díaz-Reolid, A., Aznar, R., Randazzo, W., Sánchez, G., 2022. Discrimination of non-infectious SARS-CoV-2 particles from fomites by viability RT-qPCR. Environ. Res. 203, 111831.

Davidson, J.L., Wang, J., Maruthamuthu, M.K., Dextre, A., Pascual-Garrigos, A., Mohan, S., Putikam, S.V.S., Osman, F.O.I., McChesney, D., Seville, J., Verma, M.S., 2021. A paper-based colorimetric molecular test for SARS-CoV-2 in saliva. Biosens. Bioelectron. X 9, 100076.

Dignan, L.M., Turiello, R., Layne, T.R., O'Connell, K.C., Hickey, J., Chapman, J., Poulter, M.D., Landers, J.P., 2021. An ultrafast SARS-CoV-2 virus enrichment and extraction method compatible with multiple modalities for RNA detection. Anal. Chim. Acta 1180, 338846.

Ding, L.S., Zhang, Y., Wen, D., Ma, J., Yuan, H., Li, H., Duo, S., Yuan, F., Zhang, Y.E., Zheng, A., 2022. Growth, Antigenicity, and Immunogenicity of SARS-CoV-2 spike variants revealed by a live rVSV-SARS-CoV-2 virus. Front. Med. 8.

Furukawa, N.W., Brooks, J.T., Sobel, J., 2020. Evidence supporting transmission of severe acute respiratory syndrome coronavirus 2 while presymptomatic or asymptomatic. Emerg. Infect. Dis. 26, e201595.

Gandhi, M., Yokoe, D.S., Havlir, D.V., 2020. Asymptomatic transmission, the Achilles' heel of current strategies to control Covid-19. N. Engl. J. Med. 382, 2158–2160.

GBD 2021 Demographics Collaborators, 2024. Global age-sex-specific mortality, life expectancy, and population estimates in 204 countries and territories and 811 subnational locations, 1950-2021, and the impact of the COVID-19 pandemic: a comprehensive demographic analysis for the Global Burden of Disease Study 2021. Lancet 403, 1989–2056.

Goux, H., Green, J., Wilson, A., Sozhamannan, S., Richard, S.A., Colombo, R., Lindholm, D.A., Jones, M.U., Agan, B.K., Larson, D., Saunders, D.L., Mody, R., Cox, J., Deans, R., Walish, J., Fries, A., Simons, M.P., Pollett, S.D., Smith, D.R., 2024. Performance of rapid antigen tests to detect SARS-CoV-2 variant diversity and correlation with viral culture positivity: implication for diagnostic development and future public health strategies. mBio, e0273724.

Hoffmann, M., Kleine-Weber, H., Schroeder, S., Krüger, N., Herrler, T., Erichsen, S., Schiergens, T.S., Herrler, G., Wu, N.-H., Nitsche, A., Müller, M.A., Drosten, C., Pöhlmann, S., 2020. SARS-CoV-2 cell entry depends on ACE2 and TMPRSS2 and is blocked by a clinically proven protease inhibitor. Cell 181, 271–280.e8.

Hong, W., Xiong, J., Nyaruaba, R., Li, J., Muturi, E., Liu, H., Yu, J., Yang, H., Wei, H., 2021. Rapid determination of infectious SARS-CoV-2 in PCR-positive samples by SDS-PMA assisted RT-qPCR. Sci. Total Environ. 797, 149085.

Huang, W.E., Lim, B., Hsu, C.-C., Xiong, D., Wu, W., Yu, Y., Jia, H., Wang, Y., Zeng, Y., Ji, M., Chang, H., Zhang, X., Wang, H., Cui, Z., 2020. RT-LAMP for rapid diagnosis of coronavirus SARS-CoV-2. Microb. Biotechnol. 13, 950–961.

Hurlburt, N.K., Homad, L.J., Sinha, I., Jennewein, M.F., MacCamy, A.J., Wan, Y.-H., Boonyaratanakornkit, J., Sholukh, A.M., Jackson, A.M., Zhou, P., Burton, D.R., Andrabi, R., Ozorowski, G., Ward, A.B., Stamatatos, L., Pancera, M., McGuire, A.T., 2022. Structural definition of a pan-sarbecovirus neutralizing epitope on the spike S2 subunit. Commun. Biol. 5, 1–13.

Jin, Y.-Y., Lin, H., Cao, L., Wu, W.-C., Ji, Y., Du, L., Jiang, Y., Xie, Y., Tong, K., Xing, F., Zheng, F., Shi, M., Pan, J.-A., Peng, X., Guo, D., 2021. A convenient and biosafe replicon with accessory genes of SARS-CoV-2 and its potential application in antiviral drug discovery. Virol. Sin. 36, 913–923.

Ju, B., Zhang, Q., Ge, J., Wang, R., Sun, J., Ge, X., Yu, Jiazhen, Shan, S., Zhou, B., Song, S., Tang, X., Yu, Jinfang, Lan, J., Yuan, J., Wang, H., Zhao, Juanjuan, Zhang, S., Wang, Y., Shi, X., Liu, L., Zhao, Jincun, Wang, X., Zhang, Z., Zhang, L.,

2020. Human neutralizing antibodies elicited by SARS-CoV-2 infection. Nature 584, 115–119.
Kang, T., Lu, J., Yu, T., Long, Y., Liu, G., 2022. Advances in nucleic acid amplification techniques (NAATs): COVID-19 point-of-care diagnostics as an example. Biosens. Bioelectron. 206, 114109.
Li, H., Zhang, Y., Li, D., Deng, Y.-Q., Xu, H., Zhao, C., Liu, Jiandong, Wen, D., Zhao, J., Li, Y., Wu, Y., Liu, S., Liu, Jiankai, Hao, J., Yuan, F., Duo, S., Qin, C.-F., Zheng, A., 2021. Enhanced protective immunity against SARS-CoV-2 elicited by a VSV vector expressing a chimeric spike protein. Signal Transduct. Targeted Ther. 6, 1–12.
Li, W., Moore, M.J., Vasilieva, N., Sui, J., Wong, S.K., Berne, M.A., Somasundaran, M., Sullivan, J.L., Luzuriaga, K., Greenough, T.C., Choe, H., Farzan, M., 2003. Angiotensin-converting enzyme 2 is a functional receptor for the SARS coronavirus. Nature 426, 450–454.
Li, Z., Bruce, J.L., Cohen, B., Cunningham, C.V., Jack, W.E., Kunin, K., Langhorst, B.W., Miller, J., Moncion, R.A., Poole, C.B., Premsrirut, P.K., Ren, G., Roberts, R.J., Tanner, N.A., Zhang, Y., Carlow, C.K.S., 2022. Development and implementation of a simple and rapid extraction-free saliva SARS-CoV-2 RT-LAMP workflow for workplace surveillance. PLoS One 17, e0268692.
Lin, Y., Li, Z., Wang, Y., Tian, T., Jia, P., Ye, Y., He, M., Yang, Z., Li, C., Guo, D., Hou, P., 2022. CCDC50 suppresses NLRP3 inflammasome activity by mediating autophagic degradation of NLRP3. EMBO Rep. 23, e54453.
Lu, S., Ye, Q., Singh, D., Cao, Y., Diedrich, J.K., Yates, J.R., Villa, E., Cleveland, D.W., Corbett, K.D., 2021. The SARS-CoV-2 nucleocapsid phosphoprotein forms mutually exclusive condensates with RNA and the membrane-associated M protein. Nat. Commun. 12, 502.
Mattei, S., Glass, B., Hagen, W.J.H., Kräusslich, H.-G., Briggs, J.A.G., 2016. The structure and flexibility of conical HIV-1 capsids determined within intact virions. Science 354, 1434–1437.
Meister, T.L., Dreismeier, M., Blanco, E.V., Brüggemann, Y., Heinen, N., Kampf, G., Todt, D., Nguyen, H.P., Steinmann, J., Schmidt, W.E., Steinmann, E., Quast, D.R., Pfaender, S., 2022. Low risk of severe acute respiratory syndrome coronavirus 2 transmission by fomites: a clinical observational study in highly infectious coronavirus disease 2019 patients. J. Infect. Dis. 226, 1608–1615.
Msemburi, W., Karlinsky, A., Knutson, V., Aleshin-Guendel, S., Chatterji, S., Wakefield, J., 2023. The WHO estimates of excess mortality associated with the COVID-19 pandemic. Nature 613, 130–137.
Niu, S., Wang, J., Bai, B., Wu, L., Zheng, A., Chen, Q., Du, P., Han, P., Zhang, Y., Jia, Y., Qiao, C., Qi, J., Tian, W., Wang, H., Wang, Q., Gao, G.F., 2021. Molecular basis of cross-species ACE2 interactions with SARS-CoV-2-like viruses of pangolin origin. EMBO J. 40, e107786.
Ou, X., Liu, Y., Lei, X., Li, P., Mi, D., Ren, L., Guo, L., Guo, R., Chen, T., Hu, J., Xiang, Z., Mu, Z., Chen, X., Chen, J., Hu, K., Jin, Q., Wang, J., Qian, Z., 2021. Characterization of spike glycoprotein of SARS-CoV-2 on virus entry and its immune cross-reactivity with SARS-CoV. Nat. Commun. 12, 2144.
Peeling, R.W., Heymann, D.L., Teo, Y.-Y., Garcia, P.J., 2022. Diagnostics for COVID-19: moving from pandemic response to control. Lancet 399, 757–768.
Peng, Y., Lin, C., Li, Y., Gao, Y., Wang, J., He, J., Huang, Z., Liu, J., Luo, X., Yang, Y., 2022. Identifying infectiousness of SARS-CoV-2 by ultra-sensitive SnS2 SERS biosensors with capillary effect. Matter 5, 694–709.
Plante, D., Barrera, J.A.B., Lord, M., Harlow, J., Iugovaz, I., Nasheri, N., 2024. Examining the efficiency of porcine gastric mucin-coated magnetic beads in extraction of noroviruses from frozen berries. Food Microbiol. 120, 104461.
Puente, H., Randazzo, W., Falcó, I., Carvajal, A., Sánchez, G., 2020. Rapid selective detection of potentially infectious porcine epidemic diarrhea coronavirus exposed to heat treatments using viability RT-qPCR. Front. Microbiol. 11, 1911.
Rabe, D.C., Choudhury, A., Lee, D., Luciani, E.G., Ho, U.K., Clark, A.E., Glasgow, J.E., Veiga, S., Michaud, W.A., Capen, D., Flynn, E.A., Hartmann, N., Garretson, A.F., Muzikansky, A., Goldberg, M.B., Kwon, D.S., Yu, X., Carlin, A.F., Theriault, Y., Wells, J.A., Lennerz, J.K., Lai, P.S., Rabi, S.A., Hoang, A.N., Boland, G.M., Stott, S.L., 2025. Ultrasensitive detection of intact SARS-CoV-2 particles in complex biofluids using microfluidic affinity capture. Sci. Adv. 11, eadh1167.
Rothe, C., Schunk, M., Sothmann, P., Bretzel, G., Froeschl, G., Wallrauch, C., Zimmer, T., Thiel, V., Janke, C., Guggemos, W., Seilmaier, M., Drosten, C., Vollmar, P., Zwirglmaier, K., Zange, S., Wölfel, R., Hoelscher, M., 2020. Transmission of 2019-nCoV infection from an asymptomatic contact in Germany. N. Engl. J. Med. 382, 970–971.
Selvaraj, V., Maheshwari, Y., Hajeri, S., Yokomi, R., 2019. A rapid detection tool for VT isolates of Citrus tristeza virus by immunocapture-reverse transcriptase loop-mediated isothermal amplification assay. PLoS One 14, e0222170.
Sitjar, J., Liao, J.-D., Lee, H., Tsai, H.-P., Wang, J.-R., Chen, C.-H., Wang, H., Liu, B.H., 2023. Detection of live SARS-CoV-2 virus and its variants by specially designed SERS-active substrates and spectroscopic analyses. Anal. Chim. Acta 1256, 341151.
Tan, C.W., Chia, W.N., Qin, X., Liu, P., Chen, M.I.-C., Tiu, C., Hu, Z., Chen, V.C.-W., Young, B.E., Sia, W.R., Tan, Y.-J., Foo, R., Yi, Y., Lye, D.C., Anderson, D.E., Wang, L.-F., 2020. A SARS-CoV-2 surrogate virus neutralization test based on antibody-mediated blockage of ACE2-spike protein-protein interaction. Nat. Biotechnol. 38, 1073–1078.
Tian, P., Yang, D., Jiang, X., Zhong, W., Cannon, J.L., Burkhardt, W., Woods, J.W., Hartman, G., Lindesmith, L., Baric, R.S., Mandrell, R., 2010. Specificity and kinetics of norovirus binding to magnetic bead-conjugated histo-blood group antigens. J. Appl. Microbiol. 109, 1753–1762.
Tian, P., Yang, D., Shan, L., Li, Q., Liu, D., Wang, D., 2018. Estimation of human norovirus infectivity from environmental water samples by in situ capture RT-qPCR method. Food Environ. Virol. 10, 29–38.
Veugen, J.M.J., Schoenmakers, T., van Loo, I.H.M., Haagmans, B.L., Leers, M.P.G., Lamers, M.M., Lucchesi, M., van Bussel, B.C.T., van Mook, W.N.K.A., Nuijts, R.M.M.A., Savelkoul, P.H.M., Dickman, M.M., Wolffs, P.F.G., 2024. Advancing COVID-19 diagnostics: rapid detection of intact SARS-CoV-2 using viability RT-PCR assay. Microbiol. Spectr. 12, e0016024.
V'kovski, P., Kratzel, A., Steiner, S., Stalder, H., Thiel, V., 2021. Coronavirus biology and replication: implications for SARS-CoV-2. Nat. Rev. Microbiol. 19, 155–170.
Wang, J., Shen, T., Huang, X., Kumar, G.R., Chen, X., Zeng, Z., Zhang, R., Chen, R., Li, T., Zhang, T., Yuan, Q., Li, P.-C., Huang, Q., Colonno, R., Jia, J., Hou, J., McCrae, M.A., Gao, Z., Ren, H., Xia, N., Zhuang, H., Lu, F., 2016. Serum hepatitis B virus RNA is encapsidated pregenome RNA that may be associated with persistence of viral infection and rebound. J. Hepatol. 65, 700–710.
Whitman, J.D., Hiatt, J., Mowery, C.T., Shy, B.R., Yu, R., Yamamoto, T.N., Rathore, U., Goldgof, G.M., Whitty, C., Woo, J.M., Gallman, A.E., Miller, T.E., Levine, A.G., Nguyen, D.N., Bapat, S.P., Balcerek, J., Bylsma, S.A., Lyons, A.M., Li, S., Wong, A.W.-Y., Gillis-Buck, E.M., Steinhart, Z.B., Lee, Y., Apathy, R., Lipke, M.J., Smith, J.A., Zheng, T., Boothby, I.C., Isaza, E., Chan, J., Acenas, D.D., Lee, J., Macrae, T.A., Kyaw, T.S., Wu, D., Ng, D.L., Gu, W., York, V.A., Eskandarian, H.A., Callaway, P.C., Warrier, L., Moreno, M.E., Levan, J., Torres, L., Farrington, L.A., Loudermilk, R.P., Koshal, K., Zorn, K.C., Garcia-Beltran, W.F., Yang, D., Astudillo, M.G., Bernstein, B. E., Gelfand, J.A., Ryan, E.T., Charles, R.C., Iafrate, A.J., Lennerz, J.K., Miller, S., Chiu, C.Y., Stramer, S.L., Wilson, M.R., Manglik, A., Ye, C.J., Krogan, N.J., Anderson, M.S., Cyster, J.G., Ernst, J.D., Wu, A.H.B., Lynch, K.L., Bern, C., Hsu, P.D., Marson, A., 2020. Evaluation of SARS-CoV-2 serology assays reveals a range of test performance. Nat. Biotechnol. 38, 1174–1183.
Wiersinga, W.J., Rhodes, A., Cheng, A.C., Peacock, S.J., Prescott, H.C., 2020. Pathophysiology, transmission, diagnosis, and treatment of coronavirus disease 2019 (COVID-19): a Review. JAMA 324, 782–793.
Wu, X., Liu, J., Zhang, H., Zhou, H., Wang, W., Ma, Y., Shen, S., Cai, X., Huang, A., Wang, D., 2022. Immunomolecular assay based on selective virion capture by spike antibody and viral nucleic acid amplification for detecting intact SARS-CoV-2 particles. J. Nanobiotechnol. 20, 399.
Yahalom-Ronen, Y., Tamir, H., Melamed, S., Politi, B., Shifman, O., Achdout, H., Vitner, E. B., Israeli, O., Milrot, E., Stein, D., Cohen-Gihon, I., Lazar, Shlomi, Gutman, H., Glinert, I., Cherry, L., Vagima, Y., Lazar, Shirley, Weiss, S., Ben-Shmuel, A., Avraham, R., Puni, R., Lupu, E., Bar-David, E., Sittner, A., Erez, N., Zichel, R., Mamroud, E., Mazor, O., Levy, H., Laskar, O., Yitzhaki, S., Shapira, S.C., Zvi, A., Beth-Din, A., Paran, N., Israely, T., 2020. A single dose of recombinant VSV-ΔG-spike vaccine provides protection against SARS-CoV-2 challenge. Nat. Commun. 11, 6402.
Yan, L., Zhou, J., Zheng, Y., Gamson, A.S., Roembke, B.T., Nakayama, S., Sintim, H.O., 2014. Isothermal amplified detection of DNA and RNA. Mol. Biosyst. 10, 970–1003.
Zhou, P., Yang, X.-L., Wang, X.-G., Hu, B., Zhang, L., Zhang, W., Si, H.-R., Zhu, Y., Li, B., Huang, C.-L., Chen, H.-D., Chen, J., Luo, Y., Guo, H., Jiang, R.-D., Liu, M.-Q., Chen, Y., Shen, X.-R., Wang, X., Zheng, X.-S., Zhao, K., Chen, Q.-J., Deng, F., Liu, L.-L., Yan, B., Zhan, F.-X., Wang, Y.-Y., Xiao, G.-F., Shi, Z.-L., 2020. A pneumonia outbreak associated with a new coronavirus of probable bat origin. Nature 579, 270–273.
Zhu, J., Lu, H., Lin, Q., Zhang, T., Chen, G., Zhou, Y., Sui, G., 2024. Fucoidan-based antibody-free magnetic nanoparticle for on-site detection of waterborne SARS-CoV-2. Sci. Total Environ. 911, 168619.
Zhu, Z., Guo, Y., Wang, C., Yang, Z., Li, R., Zeng, Z., Li, H., Zhang, D., Yang, L., 2023. An ultra-sensitive one-pot RNA-templated DNA ligation rolling circle amplification-assisted CRISPR/Cas12a detector assay for rapid detection of SARS-CoV-2. Biosens. Bioelectron. 228, 115179.